A Tightly Coupled Inductive Power Transfer System for Low-Voltage and High-Current Charging of Automatic Guided Vehicles

Fei Lu, *Member, IEEE*, Hua Zhang, *Member, IEEE*, Chong Zhu, *Member, IEEE*, Lijun Diao, *Senior Member, IEEE*, Minming Gong, Weige Zhang, and Chunting Chris Mi, *Fellow, IEEE*

***Abstract*—This paper proposes a tightly coupled inductive power transfer (IPT) system for the low-voltage and high-current charging of automatic guided vehicles (AGVs). There are two challenges in the system design. First, the widely varying range of the airgap introduces difficulties to design the compensation circuit. Second, the low-voltage and high-current working condition introduces difficulties to maintain the system efficiency. This paper reveals that there are a large amount of high-order harmonic currents in a tightly coupled IPT system, and we have provided an effective design method to reduce the harmonics. The integrated *LCC* compensation circuit is selected as a solution, showing four merits: good robustness to the airgap variation, easy controllability, convenience to optimize the efficiency, and low high-order harmonics. A prototype is implemented, and the magnetic coupler size is 220 × 200 × 10 mm. Experimental results show that it achieves 1.78 kW power transfer from a 300 V dc source to a 24 V battery with 86.1% efficiency and a 73.8 A charging current across an airgap of 15 mm. When the airgap varies between 5 and 25 mm, the system power variation is within ±36.7% and the efficiency is not significantly affected.**

***Index Terms*—Inductive power transfer (IPT), low-voltage and high current applications, tightly coupled.**

I. Introduction

THE loosely coupled inductive power transfer (IPT) technology has been widely applied in the charging of electric vehicles [1], [2]. The transfer distance is in the range of one hundred millimeters, which is the ground clearance of the chassis, resulting in a coupling coefficient lower than 0.30 [3], [4]. However, the system performance can be improved through the compensation circuit design, in which the *LCC* circuit is a good solution and its working principle has been analyzed [6], [7].

The study of the tightly coupled IPT technology has been started from the early 1990s [8]. The first commercial product is the GM EV1, in which a plastic paddle is inserted into an electric vehicle. However, it is not a strict "wireless" charger because a heavy cable is still required [9]. The airgap is within 10 mm, and the coupling coefficient is higher than 0.80, resulting in a tightly coupled IPT system [10], [11]. Since the paddle size perfectly matches the vehicle side space, the airgap variation is neglected, which makes its design and analysis the same as a conventional transformer. Since then, the research on the tightly coupled IPT system has been suspended due to the lack of practical applications [12], [14].

However, as shown in Fig. 1, with the rapid development of automatic guided vehicles (AGVs) in the logistics industry, it is meaningful to study its wireless charging. The transmitter is embedded on the ground side, and the receiver is installed on the AGV chassis, which provides the charging convenience. The onboard battery pack is then reduced and the effective working time is increased. The clearance of an AGV chassis is within tens of millimeters, resulting in a tightly coupled IPT system. Therefore, the study of the tightly coupled IPT technology is in an urgent demand [15], [16].

The previous research on the AGV charging focuses on the light-duty and low-power applications [17], [18]. However, in a heavy-duty application, the zero- and full-loading conditions induce a large variation of the airgap [19]. Since the ground clearance is small, the self-inductance and coupling coefficient are significantly affected. The variation can disturb the circuit

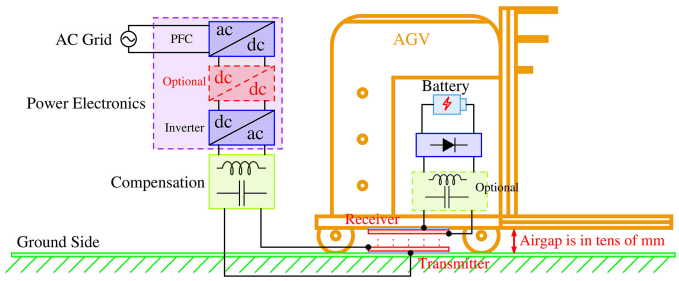

Fig. 1. Structure of a tightly coupled IPT system for automatic guided vehicle (AGV) charging.

Manuscript received April 26, 2018; revised July 31, 2018; accepted October 20, 2018. Date of publication November 15, 2018; date of current version April 30, 2019. This work was supported in part by the U.S. Department of Energy through the U.S.-China Clean Energy Center–Clean Vehicle Consortium (CERC-CVC) under Grant DE-AC02-06CH11357. *(Corresponding author: Chunting Chris Mi.)*

F. Lu and H. Zhang are with the Department of Electrical and Computer Engineering, Drexel University, Philadelphia, PA 19104 USA (e-mail: fei.lu@drexel.edu; hua.zhang@drexel.edu).

C. Zhu and C. C. Mi are with the Department of Electrical and Computer Engineering, San Diego State University, San Diego, CA 92182 USA (e-mail: chong.zhu@sdsu.edu; mi@ieee.org).

L. Diao, M. Gong, and W. Zhang are with the School of Electrical Engineering, Beijing Jiaotong University, Beijing 100044, China (e-mail: ljdiao@bjtu.edu.cn; mmgong@bjtu.edu.cn; zhangwg@dq.njtu.edu.cn).

Color versions of one or more of the figures in this paper are available online at http://ieeexplore.ieee.org.

Digital Object Identifier 10.1109/TIE.2018.2880667

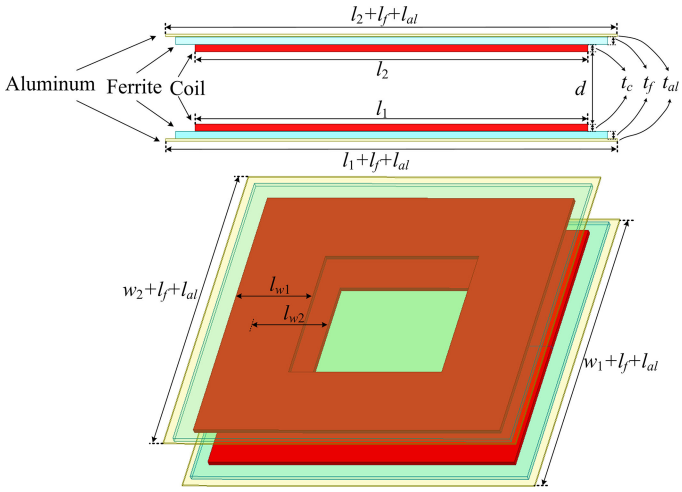

Fig. 2. Structure and dimensions of a unipolar magnetic coupler.

TABLE I
PARAMETERS DESCRIBING A UNIPOLAR MAGNETIC COUPLER

Parameter	Definition	Value
l_1, l_2, w_1, w_2	coil length and width	200 mm
l_{w1} (l_{w2})	primary (secondary) winding width	60 mm
l_f (l_{al})	length of ferrite (aluminum) edge	10 mm
t_c	coil thickness	3 mm
t_f	ferrite thickness	4 mm
t_{al}	aluminum thickness	1 mm
d	full-loading airgap	5 mm

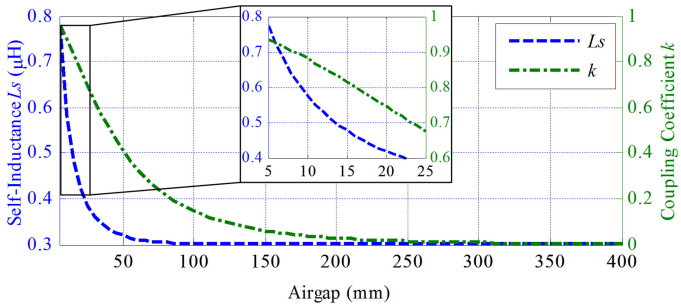

Fig. 3. Maxwell-simulated self-inductance L_s and coupling coefficient k at different airgap distances.

resonance, change the transferred power, and affect the system controllability [20], [22]. For the safe reason [23], the voltage of an AGV is usually below 60 V, and typical voltages are 12, 24, and 48 V. For example, when the voltage is 24 V and the power is 1.8 kW, the charging current can reach 75 A, resulting in a low-voltage and high-current system. The equivalent load resistance is only 0.32 Ω, which is difficult to design circuit parameters to maintain the efficiency and suppress the high-order harmonic currents [24], [25].

In this paper, the study is motivated by the challenges in a tightly coupled, low-voltage, and high-current IPT system for the AGV charging, which are summarized as two parts. First, the widely varying range of the airgap changes the inductances and coupling coefficient in a magnetic coupler and introduces difficulties to design the compensation circuit. Second, the low-voltage and high-current working condition leads to an extremely small load resistance and introduces difficulties to optimize the efficiency.

To deal with these two challenges, this paper selects the *LCC* circuit [26], [27] as a solution. It works as a current source to charge the battery, and the airgap variation does not induce a significant change in the charging power. Also, the *LCC* circuit can achieve the load resistance conversion and increase the equivalent resistance at the coil side. Therefore, it is convenient to design the coil and realize the optimal efficiency. In addition, this paper reveals the high-order harmonics problem in the *LCC* circuit and proposes an effective method to mitigate it through a proper design of circuit parameters.

II. Challenges in a Tightly Coupled, Low-Voltage, and High-Current IPT System for AGVs

In this section, the two challenges are illustrated by design examples for practical applications.

A. Widely Varying Range of the Airgap

A unipolar magnetic coupler is chosen to realize an IPT system, as shown in Fig. 2. The dimensions are shown in Table I, and the receiver size is 220 × 220 × 10 mm. In a practical system, the ground clearance of an AGV chassis is around tens of millimeters and varies in zero- and full-loading scenarios. In this example, the varying range is from 5 to 25 mm.

The finite-element analysis of the magnetic coupler is conducted in the Maxwell software, as shown in Fig. 3. The self-inductance of the one-turn coil is defined as L_s, and the coupling coefficient is defined as k.

Fig. 3 shows that both L_s and k decrease dramatically with the increasing airgap. The sensitivity of L_s and k to the airgap variation is the main difference between the tightly and loosely coupled IPT systems. In a loosely coupled system, the coil on one side is placed far from the ferrite plate on the other side, and the airgap variation has limited effect on L_s and k. However, in a tightly coupled system, the coil on one side is arranged close to the ferrite plate on the other side. When their relative position is changed, both L_s and k are significantly affected. Therefore, it is important to ensure that the power transfer process can still be maintained with a wide range of the airgap variation. This target is the first challenge in designing a tightly coupled IPT system for the AGV charging application.

B. Efficiency Optimization With Low Voltage and High Current

The general structure of an IPT system is shown in Fig. 4, where L_1 and L_2 are the self-inductances. The angular resonant frequency is ω_0, the quality factors of the primary and secondary circuits are Q_1 and Q_2, and the equivalent load resistance is defined as $R_{\rm eq}$. The ratio between $R_{\rm eq}$ and the impedance of L_2

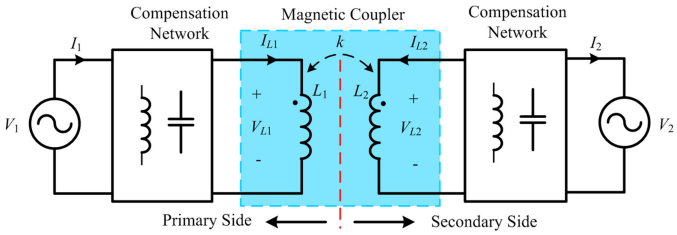

Fig. 4. General structure of an IPT system.

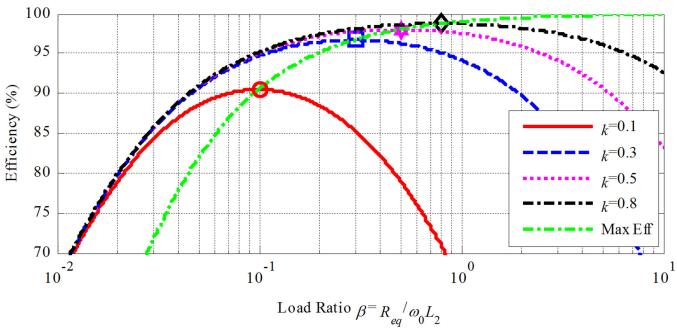

Fig. 5. Efficiency of the resonant circuit at different k and load ratio β when $Q = 200$.

is defined as β, which is expressed as follows:

$$\beta = \frac{R_{\mathrm{eq}}}{\omega_0 L_2}. \tag{1}$$

According to [5], the transfer efficiency η of the resonant circuit is calculated as follows:

$$\eta = \frac{1}{1 + \frac{1}{\beta Q_2} + \left(\beta Q_2 + \frac{1}{\beta Q_2} + 2\right) \cdot \frac{1}{k^2 Q_1 Q_2}}. \tag{2}$$

Assuming $Q = Q_1 = Q_2 = 200$ as an example, η is calculated at different k and β, as shown in Fig. 5. It shows that, for a specific coupling coefficient k, there is an optimal β that can maximize the efficiency. According to (2), this optimal β is expressed as follows:

$$\beta_{\eta\,\max} = \sqrt{(1 + k^2 Q_1 Q_2)}/Q_2. \tag{3}$$

Since $kQ \gg 1$, the optimal load resistance $R_{\mathrm{eq},\eta\max}$ is given as follows:

$$R_{\mathrm{eq},\eta\,\max} = k \cdot \omega_0 L_2. \tag{4}$$

It means the optimal equivalent load resistance $R_{\mathrm{eq},\eta\max}$ is equal to the product of k and the impedance of L_2. Then, in a tightly coupled IPT system, a relatively large k requires a large $R_{\mathrm{eq},\eta\max}$ to obtain the maximum efficiency. However, in the low-voltage and high-current application, the equivalent load resistance is very small (even less than 1.0 Ω). As a result, the secondary self-inductance L_2 should be extremely small to optimize the efficiency, which is difficult to achieve in practice. Therefore, the efficiency optimization in the low-voltage and high-current condition is the second challenge in the design of an AGV charging system.

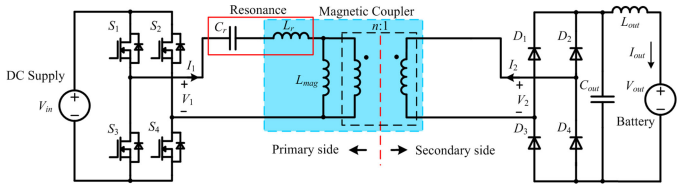

Fig. 6. Circuit topology of a tightly coupled IPT system based on the *LLC* resonant converter.

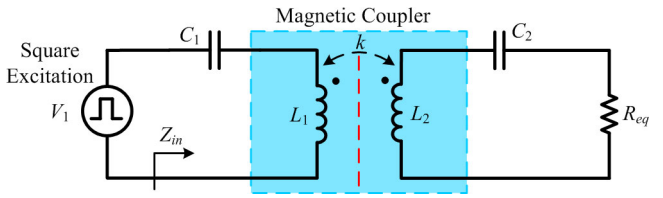

Fig. 7. Equivalent circuit model of a tightly coupled IPT system based on series–series compensation.

III. Solution-Integrated LCC Compensation

There are mainly three categories of compensation circuits for an IPT system. First, only one capacitor is added, which is the *LLC* converter. Second, two capacitors are added, in which the series–series (SS) circuit has been widely applied. Third, three or more components are added, and the double-sided *LCC* circuit is a good solution. These three compensation circuits are analyzed in detail as follows.

A. LLC Converter

The *LLC* converter with a tightly coupled transformer is shown in Fig. 6, and the parameter relationship is given as follows:

$$\begin{cases} L_{\mathrm{mag}} = k^2 \cdot L_1, n = k \cdot \sqrt{L_1/L_2} \\ L_r = (1 - k^2) \cdot L_1, C_r = 1/(\omega_0^2 \cdot L_r) \end{cases}. \tag{5}$$

According to [28], the capacitor C_r is used to compensate the leakage inductance L_r, resulting in a constant-voltage working mode. Meanwhile, the output power can be regulated through tuning the switching frequency.

However, the disadvantage is that the *LLC* converter cannot achieve wireless charging when there is a large airgap variation. Since the *LLC* resonant converter works in a constant-voltage mode, the parameter variation can lead to a dramatic increase in the charging current, which is dangerous. Then, an additional control mechanism should be applied to protect the charging system, but the response speed and reliability are two demanding requirements. Besides, the system cost and complexity are increased as well.

B. Series–Series Compensation

The SS compensation is shown in Fig. 7, including a square wave input source and an equivalent resistor R_{eq}. The resonant relationship is $L_1 C_1 = L_2 C_2 = 1/\omega_0^2$. Since it works as a current source [29], it is less sensitive to the airgap variation.

TABLE II
REAL AND IMAGINARY PARTS OF Z_{in} AT DIFFERENT FREQUENCIES

Harmonics	Re(Z_{in})	Im(Z_{in})
1	R_1	0
3	$R_1 \cdot \frac{81k^2}{64+9k^2}$	$R_1 \cdot \frac{1}{k} \cdot \frac{8}{9} \cdot \frac{64-72k^2}{64+9k^2}$
5	$R_1 \cdot \frac{625k^2}{576+25k^2}$	$R_1 \cdot \frac{1}{k} \cdot \frac{24}{25} \cdot \frac{576-600k^2}{576+25k^2}$
n	$R_1 \cdot \frac{n^4k^2}{(n^2-1)^2+n^2k^2}$	$R_1 \cdot \frac{1}{k} \cdot \frac{n^2-1}{n^2} \cdot \frac{(n^2-1)^2-n^2(n^2-1)k^2}{(n^2-1)^2+n^2k^2}$

The input voltage V_1 contains high-order harmonics (third, fifth, seventh, ...) expressed as follows:

$$V_1 = |V_{\text{in}}| \cdot \frac{4}{\pi} \cdot \left(\sin \omega_0 t + \frac{1}{3} \sin 3\omega_0 t + \frac{1}{5} \sin 5\omega_0 t + \frac{1}{7} \sin 7\omega_0 t + \cdots \right). \quad (6)$$

At a specific frequency ω, the input-side impedance Z_{in} in Fig. 7 is calculated as follows (7) shown at the bottom of this page.

Generally, the system parameters are designed to maximize the efficiency. Therefore, (4) is substituted into (7) to acquire the impedance Z_{in} at the frequency $\omega_n = n\omega_0$ $(n = 1, 3, 5, 7 \ldots)$ shown as follows (8) shown at the bottom of this page.

At the fundamental frequency $\omega_1 = \omega_0$, the impedance only contains a real part, which is defined as R_1:

$$R_1 = Z_{\text{in}}(\omega_1) = \omega_0 L_1 \cdot k. \quad (9)$$

Then, the real and imaginary parts of Z_{in} are calculated in Table II. Since $n^2 \gg 1$ when $n = 3, 5, 7 \ldots$, Z_{in} is approximated as follows:

$$\begin{cases} Z_{\text{in}}(\omega_1) = R_1, n = 1 \\ Z_{\text{in}}(\omega_n) \approx R_1 \cdot k^2 + jR_1 \cdot \dfrac{1-k^2}{k}, n = 3, 5, 7, \ldots \end{cases}. \quad (10)$$

According to Table II, the normalized magnitude $|Z_{\text{in}}|/R_1$ is calculated in Fig. 8. Based on (10), the generalized value of $|Z_{\text{in}}|/R_1$ is also provided as a red-solid curve for comparison.

Fig. 8 shows that, at the high-order harmonic frequencies, Z_{in} is determined by k. In a loosely coupled IPT system with a low k, $|Z_{\text{in}}|$ is much higher than R_1 at high frequencies, which can reduce the harmonic currents. However, in a tightly coupled system with a high k, $|Z_{\text{in}}|$ is smaller than R_1 at high frequencies.

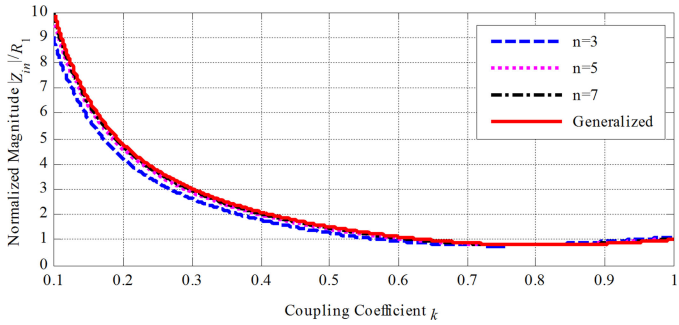

Fig. 8. Normalized magnitude $|Z_{\text{in}}|/R_1$ at different coupling coefficient k for different high-order harmonic frequencies.

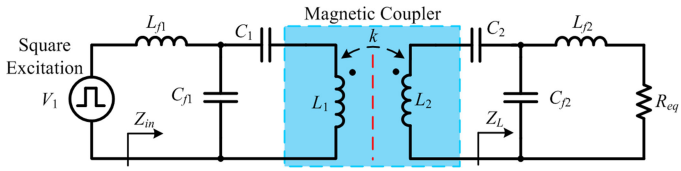

Fig. 9. Equivalent circuit model of a tightly coupled IPT system based on *LCC—LCC* compensation.

Then, there are harmonic currents that affect the soft-switching condition and induce extra power losses.

C. Integrated LCC Compensation

The circuit topology of a double-sided *LCC* circuit is shown in Fig. 9. The parameter relationship is expressed as follows:

$$\begin{cases} \omega_0^2 \cdot L_{f1}C_{f1} = \omega_0^2 \cdot L_{f2}C_{f2} = 1 \\ \omega_0^2 \cdot (L_1 - L_{f1}) \cdot C_{f1} = \omega_0^2 \cdot (L_2 - L_{f2}) \cdot C_{f2} = 1 \end{cases}. \quad (11)$$

According to [6], the *LCC* circuit works as a current source, and it is less sensitive to the airgap variation, which is an advantage over the voltage-source converter. In this way, it can solve the challenge presented in Section II-A.

At the fundamental frequency ω_0, the equivalent load impedance Z_L is calculated as follows:

$$Z_L = R_L + jX_L = Q_L^2 R_{\text{eq}} + \frac{1}{j\omega_0 C_{f2}} \quad (12)$$

where $Q_L = \omega_0 L_{f2}/R_{\text{eq}}$ is the load side quality factor. In a low-voltage and high-current system, since R_{eq} is very small, Q_{L} is then very large. The resistance R_L is much larger than R_{eq}. Considering the optimal efficiency condition in (4), the optimal L_2 is increased, which realizes the optimal efficiency

$$Z_{\text{in}}(\omega) = \frac{L_1}{L_2} \cdot R_{\text{eq}} \cdot \frac{k^2\omega^2 L_2^2}{R_{\text{eq}}^2 + \omega^2 L_2^2 \cdot \left(1 - \frac{\omega_0^2}{\omega^2}\right)^2} + j\omega L_1 \cdot \left(1 - \frac{\omega_0^2}{\omega^2}\right) \cdot \left(1 - \frac{k^2\omega^2 L_2^2}{R_{\text{eq}}^2 + \omega^2 L_2^2 \cdot \left(1 - \frac{\omega_0^2}{\omega^2}\right)^2}\right). \quad (7)$$

$$Z_{\text{in}}(\omega_n) = \omega_0 L_1 \cdot \frac{n^4 k^3}{n^2k^2 + (n^2-1)^2} + j\omega L_1 \cdot \frac{n^2-1}{n^2} \cdot \frac{(n^2-1)^2 - n^4k^2 + n^2k^2}{n^2k^2 + (n^2-1)^2}, n = 1, 3, 5, 7 \ldots \quad (8)$$

and a reasonable value of L_2 simultaneously. In this way, it can solve the challenge presented in Section II-B.

At the high-order harmonic frequencies $\omega_n = n\omega_0\,(n = 3, 5, 7\ldots)$, the impedance $1/(\omega_n C_{f2})$ is much smaller than $(\omega_n L_{f2} + R_{\text{eq}})$. Then, Z_{in} is approximated as follows:

$$Z_{\text{in}} = j\omega_0 L_{f1} \cdot n \cdot \left(1 - \frac{1}{n^2}\right) \cdot \frac{\left[\left(1 - \frac{1}{n^2}\right)^2 - \frac{L_{f1}/L_1}{n^4}\right] - k^2}{\left(1 - \frac{1}{n^2}\right)^2 - k^2},$$
$$n = 3, 5, 7\ldots \tag{13}$$

It shows that there exists a critical coupling coefficient k_n that can induce a high-order harmonic current:

$$k_n = \sqrt{\left(1 - \frac{1}{n^2}\right)^2 - \frac{L_{f1}/L_1}{n^4}}, n = 3, 5, 7\ldots \tag{14}$$

If $L_{f1} = L_1$ is taken as an example, (14) shows when k is 0.882, 0.959, and 0.979, the third, fifth, and seventh harmonics are maximized, respectively, which can cause a severe current distortion.

According to the previous analysis, the harmonic currents are increased when two conditions are satisfied simultaneously: first, the parameters follow the resonant relationship in (11); second, k reaches the singular value in (14). In a tightly coupled system, it is unavoidable to satisfy (14) as the airgap decreases. For example, when the airgap is between 25 and 5 mm, k varies between 0.68 and 0.92. Therefore, this paper proposes to reduce the harmonic currents by detuning the parameters, which means (11) cannot be satisfied when k follows (14).

For example, the circuit resonance can be designed at a k value of 0.80, which is lower than 0.882. When the airgap decreases, k approaches 0.882, and (14) is satisfied. However, since the inductances are increased, (11) is no longer satisfied. In this way, the harmonic currents are reduced.

The relative increase ratio of inductance is defined as δ_L. Then, Z_{in} is rewritten as follows (15) shown at the bottom of this page.

The impedance of L_{f1} is defined as $Z_{Lf1} = j\omega_0 L_{f1}$. Then, the normalized magnitude $|Z_{\text{in}}|/|Z_{\text{Lf1}}|$ is compared for the third and fifth harmonic frequencies with or without the inductance variations, as shown in Fig. 10. If there is no inductance variation ($\delta_L = 0$), Z_{in} decreases to zero at $k = 0.882$ for the third harmonic and $k = 0.959$ for the fifth harmonic, which can induce significant harmonic currents. However, when there is a 20% inductance variation ($\delta_L = 0.2$), Z_{in} is increased and the harmonic currents are reduced.

The *LCC* circuit has two advantages over the SS circuit. First, it is convenient to optimize the efficiency. The conversion of the equivalent load resistance provides a wider range to design L_2 in a low-voltage and high-current system. Second, the *LCC* circuit can reduce the harmonic currents. An *LCC*-compensated system only has one high-order harmonic current at a particular

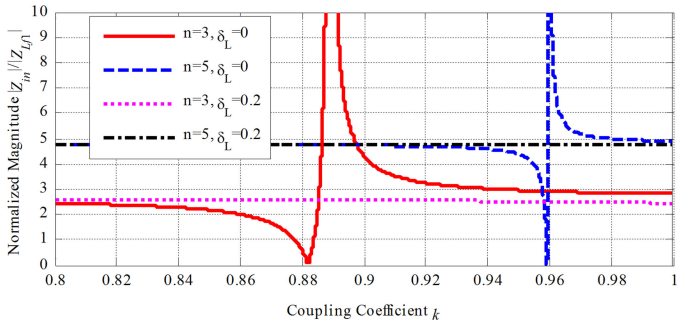

Fig. 10. Normalized magnitude $|Z_{\text{in}}|/|Z_{\text{Lf1}}|$ at different k for third and fifth harmonics frequencies with and without inductance variations.

TABLE III
SPECIFICATIONS OF A TIGHTLY COUPLED IPT SYSTEM FOR AGVs

Parameter	Design Value	Parameter	Design Value
V_{in}	300 V	V_{out}	24 V
f_{sw}	85 kHz	k	0.68~0.92
L_{f1}	110 μH	L_{f2}	3.26 μH
C_{f1}	31.9 nF	C_{f2}	1073.9 nF
L_1	150 μH	L_2	45 μH
C_1	87.6 nF	C_2	84.0 nF

k, and it can be reduced by the parameter design. In addition, the compensation inductors can be integrated into the main coils to save space, resulting in the integrated *LCC* compensation [26], [27].

The analysis of the tightly coupled IPT system is the main contribution of this paper, which reveals the differences between the loosely and tightly coupled IPT systems. It points out that the harmonic currents can be very significant when k is high. Also, the harmonic currents can be reduced by detuning the parameters, which provides the guideline to design a tightly coupled IPT system.

IV. LCC COMPENSATION BASED EXAMPLE

A. Circuit Parameters Design

A 1.8 kW tightly coupled IPT system is designed with the circuit parameters in Table III.

The input voltage is 300 V, and the battery voltage is 24 V. Under different loading conditions, d varies between 5 and 25 mm. The middle position ($d = 15$ mm) is selected to design the capacitances, and the coupling coefficient k is 0.80. According to Section III-C, L_{f1} can help reduce the harmonic currents, and it is 110 μH in this design. Considering the limited space at the vehicle side, L_{f2} is 3.4 μH. Based on (4) and (12), L_2 is selected to optimize the efficiency. Then, L_1 is 150 μH and L_2 is 45 μH, which can also limit the current density within 6 A/m^2.

$$Z_{\text{in}} = j\omega_0 L_{f1} \cdot n \cdot \left(1 - \frac{1}{n^2}\right) \cdot \frac{\left[\left(1 + \delta_L - \frac{1}{n^2}\right)^2 - \frac{L_{f1}/L_1}{n^4} \cdot \left(1 + \delta_L \cdot \frac{n^2}{n^2 - 1}\right)\right] - k^2}{\left(1 + \delta_L - \frac{1}{n^2}\right)^2 - k^2}, n = 3, 5, 7\ldots \tag{15}$$

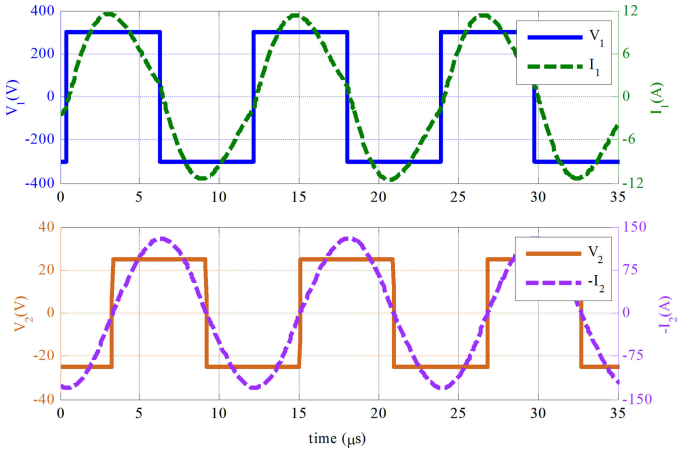

Fig. 11. LTspice-simulated input and output waveforms of voltages and currents.

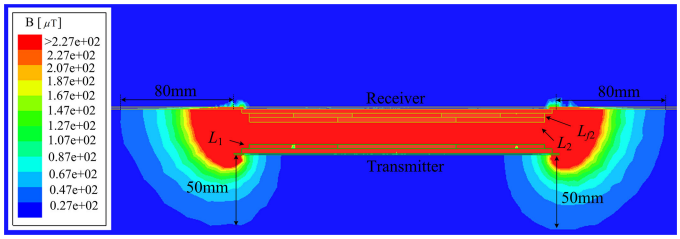

Fig. 12. Finite-element analyzed magnetic field emission of a tightly coupled magnetic coupler at 1.8 kW output power.

B. Simulation Results

The circuit is simulated in the LTspice software, as shown in Fig. 11. The unity power factor condition is achieved, which limits the reactive power. The cut-off current at the switching transient is positive, which achieves the zero-voltage-switching condition [6]. The current waveforms are close to the pure sinusoidal forms, and the harmonic components are limited. The total harmonic distortion of I_1 is 8.4%, which is mainly induced by the third-order harmonic.

The FEM analysis of the magnetic field emission is conducted in the Maxwell software and shown in Fig. 12. The vehicle chassis is considered as a shielding plate, and its size is chosen as 500 $\times$ 500 mm. Since the space on the vehicle side is limited, L_{f2} is integrated into L_2. Based on the ICNIRP 2010 requirement, the magnetic field strength should be lower than 27 μT [30]. The simulation result shows that the safe range of this 1.8 kW IPT system is 80 mm away from the magnetic coupler. Considering the size of a practical AGV system, it is safe for a human to appear close to the charging area when it is in the operation status.

V. Experimental Demonstration

A. Prototype Implementation

According to Tables I and III, a prototype of the magnetic coupler is constructed. The 3000-strand AWG 46 Litz wire is used to make coils. Measurements show that the quality factor of L_{f2} is 240, which is acceptable in a practical design. In the design, L_1 has 20 turns, L_2 has 14 turns, and L_{f2} has 2 turns to achieve the required inductance.

An inverter with MOSFETs (C2M0025120D) is used at the input side, and low-loss Schottky diodes (DSSK40-008B) are used in the rectifier. At the output side, an electronic load in the constant-voltage mode is used to emulate the battery.

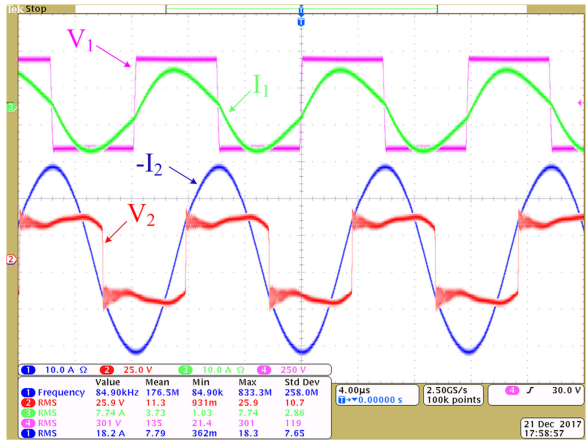

Fig. 13. Experimental waveforms when the airgap is 15 mm.

TABLE IV
Power Loss Breakdown Among the Components in the Circuits

Rectifier	$P_{Lf1,2}$	$P_{Cf1,2}$	$P_{L1,2}$	$P_{C1,2}$	Inverter
44%	25%	14%	12%	3%	2%

B. Experimental Results at 15 mm Airgap

When the airgap is 15 mm, the experimental waveforms are shown in Fig. 13.

The experimental waveforms are similar to the simulation results. At the input side, the soft-switching condition is achieved for the MOSFETs. At the output side, since the magnitude of the output current ($-I_2$) exceeds the range of the probe, only one-sixth of ($-I_2$) is measured. The waveforms also show a slight phase difference between V_2 and ($-I_2$), which is caused by the parasitic capacitances of the diodes.

When the input voltage reaches 300 V and the output voltage reaches 24 V, the input power is 2.06 kW and the output power is 1.78 kW, resulting in a dc–dc efficiency of 86.1% from the dc source to the dc load. In this case, the charging current to the battery is 73.8 A, which validates the low-voltage and high-current design.

Based on the measured quality factor and the datasheets of the components, the power loss breakdown is shown in Table IV. Due to the large output current, the rectifier dissipates 44% of the total loss. The forward voltage of the diode is 0.68 V at 40 A current. In the future design, better diodes or synchronous rectification may be adopted to further improve the efficiency. Since the current density in the main coils is limited in this design, the power loss in L_1 and L_2 is also limited, which is only 12% of the total loss. However, because of the high output current, the power loss in L_{f2} is high, and it can be reduced by using thicker wire and more magnetic materials.

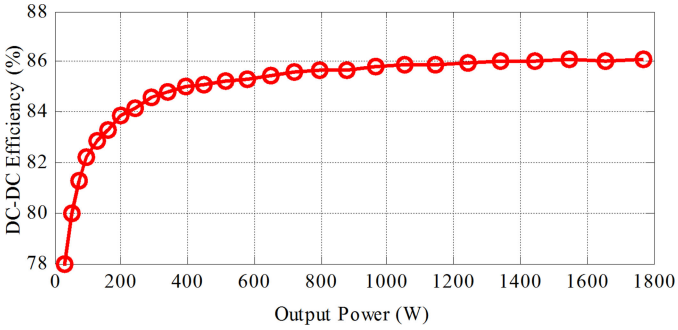

Fig. 14. Experimental power and efficiency when the airgap is 15 mm.

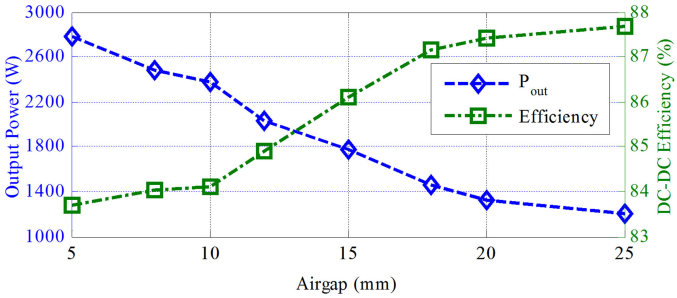

Fig. 15. Experimental output power and efficiency when the airgap varies.

When the airgap is 15 mm, the system efficiency is also measured at different output powers, as shown in Fig. 14. It indicates that the designed system can maintain a relatively high efficiency over a large range of the output power. For example, as long as the power reaches one-third of the nominal value, the system efficiency is higher than 85%.

C. Experimental Results With Airgap Variation

Under different loading conditions, the airgap varies, and the output power and efficiency are measured in Fig. 15.

When the airgap decreases to 5 mm, k is 0.92 and the output power reaches 2.70 kW. Since the magnetic field strength in the magnetic coupler increases, the power loss also increases and the efficiency decreases to 83.8%. When the airgap increases to 25 mm, k is 0.68 and the output power is 1.25 kW. Since the magnetic loss is reduced, the efficiency increases to 87.8%. Therefore, the variation of the efficiency is within ±2.0%, and the relative variation of the output power δ_P is calculated as follows:

$$\delta_P = \left|\frac{P_{\max} - P_{\min}}{P_{\max} + P_{\min}}\right| \times 100\% = 36.7\%. \tag{16}$$

Therefore, when the airgap varies from 5 to 25 mm, as long as the input voltage is controlled within ±36.7% of its nominal value, the constant-current charging profile can be achieved without significantly affecting the efficiency.

When the airgap varies, the currents I_{L1} and I_{L2} of the main coils are measured. Experimental results show that the distortion of I_{L2} can be neglected. However, the distortion of I_{L1} can be very significant. Therefore, the experimental waveforms of the primary current I_{L1} are shown in Fig. 16. When the airgap is small (for example, $d = 5$ and 8 mm), the distortion of I_{L1} is very obvious. When the airgap increases (for example, $d = 15$ and 25 mm), the distortion of I_{L1} is reduced.

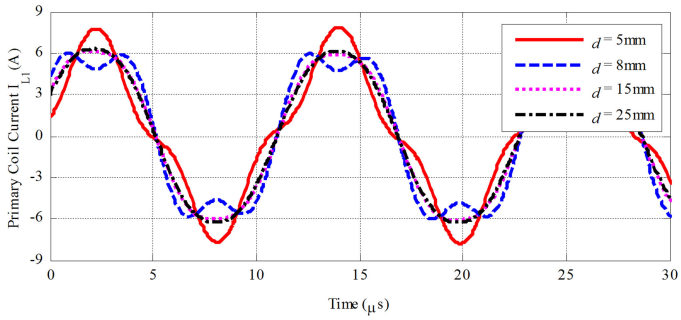

Fig. 16. Experimental waveforms of I_{L1} when the airgap varies.

TABLE V
FFT ANALYSIS OF THE PRIMARY COIL CURRENT I_{L1} WHEN THE AIRGAP VARIES

airgap \ harmonic	3rd	5th	7th	9th
5 mm	21.9%	1.3%	0.2%	0.1%
10 mm	24.7%	0.8%	0.2%	0.1%
15 mm	6.7%	0.4%	0.1%	0.06%
25 mm	3.5%	0.3%	0.1%	0.05%

A further analysis of I_{L1} using fast Fourier transform (FFT) is performed in Table V. It indicates that the third harmonic current dominates the total distortion, which validates the analysis in Section III-C. When the airgap varies between 5 and 25 mm, the worst case appears around 8 mm (the measured $k = 0.90$), and the distortion is about 24.7%. If the airgap increases to 15 mm, the distortion is only 6.7%, which validates that the *LCC* circuit could achieve a relatively low distortion.

VI. Conclusion

This paper aimed at the tightly coupled inductive charging of the AGV. Compared to a loosely coupled system, the proposed system had two distinguishing challenges: the wide range of airgap variation and the low-voltage and high-current output property. Also, this paper revealed that a tightly coupled system could generate a large amount of high-order harmonic currents. Therefore, this paper adopted the *LCC* compensation circuit to deal with the challenges, and a prototype was implemented. The magnetic coupler size was 220 × 220 × 10 mm for a practical AGV application. For the first challenge, when the airgap varied between 5 and 25 mm, the relative variation of the output power was within ±36.7%, and the system efficiency was not significantly affected. For the second challenge, it achieved 1.78 kW power transfer to a 24 V battery with a charging current as high as 73.8 A. Meanwhile, the distortion of the coil current was limited to 24.7%.

References

[1] S. Y. R. Hui, "Past, present and future trends of non-radiative wireless power transfer," *CPSS Trans. Power Electron. Appl.*, vol. 1, no. 1, pp. 83–91, 2016.

[2] G. A. Covic, and J. T. Boys, "Inductive power transfer," *Proc. IEEE*, vol. 101, no. 6, pp. 1276–1289, Jun. 2013.
[3] C. J. Chen, T. H. Chu, C. L. Lin, and Z. C. Jou, "A study of loosely coupled coils for wireless power transfer," *IEEE Trans. Circuits Syst. II: Express Briefs*, vol. 57, no. 7, pp. 536–540, Jul. 2010.
[4] F. Lu, H. Zhang, H. Hofmann, and C. Mi, "A high efficiency 3.3 kW loosely-coupled wireless power transfer system without magnetic material," in *Proc. IEEE Energy Convers. Congr. Expo.*, 2015, pp. 2282–2286.
[5] S. Li and C. Mi, "Wireless power transfer for electric vehicle applications," *IEEE J. Emerging Sel. Top. Power Electron.*, vol. 3, no. 1, pp. 4–17, Mar. 2015.
[6] S. Li, W. Li, J. Deng, T. Nguyen, and C. Mi, "A double-sided LCC compensation network and its tuning method for wireless power transfer," *IEEE Trans. Veh. Technol.*, vol. 64, no. 6, pp. 2261–2273, Jun. 2015.
[7] J. Deng, F. Lu, S. Li, T. D. Nguyen, and C. Mi, "Development of a high efficiency primary side controlled 7 kW wireless power charger," in *Proc. IEEE Int. Electr. Veh. Conf.*, 2014, pp. 1–6.
[8] K. W. Klontz, A. Esser, and R. R. Bacon, "An electric vehicle charging system with universal inductive interface," in *Proc. IEEE Power Convers. Conf.*, 1993, pp. 227–232.
[9] "Society of automotive engineering recommended practice for electric vehicle inductively coupled charging," SAE recommended practice, 1999.
[10] J. Hirai, E. W. Kim, and A. Kawamura, "Study on intelligent battery charging using inductive transmission of power and information," *IEEE Trans. Power Electron.*, vol. 15, no. 2, pp. 335–345, Mar. 2000.
[11] M. G. Egan, D. L. Sullivan, J. G. Hayes, M. J. Willers, and C. P. Henze, "Power factor corrected single stage inductive charger for electric vehicle batteries," *IEEE Trans. Ind. Electron.*, vol. 54, no. 2, pp. 1217–1226, Apr. 2007.
[12] C. Song *et al.*, "Low EMF and EMI design of a tightly coupled handheld resonant magnetic field (HH-RMF) charger for automotive battery charging," *IEEE Trans. Electromagn. Compat.*, vol. 58, no. 4, pp. 1194–1206, Aug. 2016.
[13] K. Yoon, C. Song, H. Kim, Y. Cho, S. Jeong, and J. Kim, "Reduction method of electromagnetic interference in tightly-coupled resonant magnetic field automotive charger with input impedance design," in *Proc. IEEE Wireless Power Transf. Conf.*, 2016, pp. 1–3.
[14] I. G. Sirbu, A. Marinescu, and L. Mandache, "On electric vehicle wireless chargers with tight coupling," in *Proc. Int. Symp. Adv. Top. Electr. Eng.*, 2017, pp. 404–409.
[15] S. Berman, Y. Edan, and M. Jamshidi, "Navigation of decentralized autonomous automatic guided vehicles in material handling," *IEEE Trans. Robot. Autom.*, vol. 19, no. 4, pp. 743–749, Aug. 2003.
[16] "Battery charging systems for automated guided vehicles," AGV Battery Charging Syst., Egemin Autom. Inc., Holland, MI, USA, 2016.
[17] H. Matsumoto, Y. Shibako, and Y. Neba, "Contactless power transfer system for AGVs," *IEEE Trans. Ind. Electron.*, vol. 65, no. 1, pp. 251–260, Jan. 2018.
[18] A. Zaheer, G. A. Covic, and D. Kacprzak, "A bipolar pad in a 10 kHz 300-W distributed IPT system for AGV applications," *IEEE Trans. Ind. Electron.*, vol. 61, no. 7, pp. 3288–3301, Jul. 2014.
[19] C. Zheng, H. Ma, J. S. Lai, and L. Zhang, "Design consideration to reduce gap variation and misalignment effect for the inductive power transfer system," *IEEE Trans. Power Electron.*, vol. 30, no. 11, pp. 6108–6119, Nov. 2015.
[20] C. S. Wang, G. A. Covic, and O. H. Stielau, "Power transfer capability and bifurcation phenomena of loosely coupled inductive power transfer systems," *IEEE Trans. Ind. Electron.*, vol. 51, no. 1, pp. 148–157, Feb. 2004.
[21] X. Dai, Y. Sun, C. Tang, Z. Wang, Y. Su, and Y. Li, "Dynamic parameters identification method for inductively coupled power transfer system," in *Proc. IEEE Int. Conf. Sustain. Energy Technol.*, 2010, pp. 1–5.
[22] F. Lu, H. Hofmann, J. Deng, and C. Mi, "Output power and efficiency sensitivity to circuit parameter variations in double-sided LCC-compensated wireless power transfer system," in *Proc. IEEE Appl. Power Electron. Conf. Expo.*, 2015, pp. 597–601.
[23] P. J. Grbovic, F. Crescimbini, A. Lidozzi, and L. Solero, "Multi-level converters for low voltage high current applications: Issues, challenges and limitations," in *Proc. Int. Power Electron. Motion Control Conf. Expo.*, 2014, pp. 737–744.
[24] U. Schwalbe, M. Schilling, B. Koehnlechner, and T. Reimann, "Challenges in low-voltage high-current applications - Fathom the limits in system design," in *Proc. Int. Conf. Integr. Power Electron.*, 2016, pp. 1–7.
[25] X. Duan and A. Q. Huang, "Current-mode variable-frequency control architecture for high-current low-voltage dc-dc converters," *IEEE Trans. Power Electron.*, vol. 21, no. 4, pp. 1133–1137, Jul. 2006.
[26] J. Deng, F. Lu, W. Li, R. Ma, and C. Mi, "ZVS double-side LCC compensated resonant inverter with magnetic integration for electric vehicle wireless charger," in *Proc. IEEE Appl. Power Electron. Conf. Expo.*, 2015, pp. 1131–1136.
[27] F. Lu, H. Zhang, H. Hofmann, W. Su, and C. Mi, "A dual-coupled LCC-compensated IPT system with a compact magnetic coupler," *IEEE Trans. Power Electron.*, vol. 33, no. 7, pp. 6391–6402, Jul. 2018.
[28] J. Deng, S. Li, S. Hu, C. Mi, and R. Ma, "Design methodology of LLC resonant converters for electric vehicle battery chargers," *IEEE Trans. Veh. Technol.*, vol. 63, no. 4, pp. 1581–1592, May 2014.
[29] W. Zhang, S. C. Wong, C. K. Tse, and Q. Chen, "Design for efficiency optimization and voltage controllability of series–series compensated inductive power transfer systems," *IEEE Trans. Power Electron.*, vol. 29, no. 1, pp. 191–200, Jan. 2014.
[30] "ICNIRP guidelines for limiting exposure to time-varying electric, magnetic and electromagnetic fields (1 Hz to 100 kHz)," *Health Phys.*, vol. 99, pp. 818–836, 2010.

Fei Lu (S'12–M'17) received the B.S. and M.S. degrees from the Harbin Institute of Technology, Harbin, China, in 2010 and 2012, respectively, and the Ph.D. degree from the University of Michigan, Ann Arbor, MI, USA, in 2017, all in electrical engineering.

He is currently an Assistant Professor with the Department of Electrical and Computer Engineering, Drexel University, Philadelphia, PA, USA. His research interests include power electronics and the application of electric vehicle charging.

Hua Zhang (S'14–M'17) received the B.S., M.S., and Ph.D. degrees in electrical engineering from Northwestern Polytechnical University, Xi'an, China, in 2011, 2014, and 2017, respectively.

From September 2014 to August 2015, she was a joint Ph.D. student founded by the China Scholarship Council with the University of Michigan, Dearborn, MI, USA. From September 2015, she started to work with San Diego State University. She is currently a Postdoctoral Research Associate with Drexel University, Philadelphia, PA, USA. Her research interest focuses on the charging technology of electric vehicles.

Chong Zhu (M'17) received the B.S. degree from China University of Mining and Technology, Xuzhou, China, in 2010, and the Ph.D. degree from Zhejiang University, Hangzhou, China, in 2016, both in electrical engineering.

He is currently a Postdoctoral Researcher with San Diego State University, San Diego, CA, USA. His research interests include battery thermal management, ac–dc power conversion, and pulsewidth modulation techniques applied in electric vehicles.

Lijun Diao (M'10–SM'18) received the B.Eng. and Ph.D. degrees in electrical engineering from Beijing Jiaotong University, Beijing, China, in 2003 and 2008, respectively.

He is currently the Vice-Dean of Beijing Engineering Research Center for Electrical Rail Transit. He was the PI of the traction systems' R&D for China's first 100% low floor light rail vehicle and first hybrid EMU. His research interests include power electronics and ac drives, transportation and ship electrification applications, hybrid energy management, and safety control.

Minming Gong received the B.Eng. and M.Eng. degrees in electrical engineering from Beijing Jiaotong University, Beijing, China, in 1994 and 2008, respectively.

He is currently a Senior Engineer with the School of Electrical Engineering, Beijing Jiaotong University, and the Vice-Dean of the National Active Distribution Network Technology Research Center. His research interest focuses on applications of lithium battery group technology and new energy.

Weige Zhang received the M.S. and Ph.D. degrees in electrical engineering from Beijing Jiaotong University, Beijing, China, in 1997 and 2013, respectively.

He is currently a Professor with the School of Electrical Engineering, Beijing Jiaotong University. His research interests include battery pack application technology, power electronics, and intelligent distribution system.

Chunting Chris Mi (S'00–A'01–M'01–SM'03–F'12) received the B.S.E.E. and M.S.E.E. degrees from Northwestern Polytechnical University, Xi'an, China, in 1985 and 1988, respectively, and the Ph.D. degree from the University of Toronto, Toronto, ON, Canada, in 2001, all in electrical engineering.

He is a Professor and the Chair of electrical and computer engineering and the Director of the Department of Energy-Funded Graduate Automotive Technology Education Center for Electric Drive Transportation, San Diego State University (SDSU), San Diego, CA, USA. Prior to joining SDSU, he was with the University of Michigan, Dearborn, from 2001 to 2015.